SCIENCEFORECAST
A digital science library

Research Article
Published: 26 Jan, 2018

SF Journal of Material and Chemical Engineering

Development of Robust Tri-Bore Hollow Fiber Membranes for the Control of Dissolved Oxygen in Water

*Mao L, Wang F and Su J**

School of Life Sciences & Chemical Technology, Ngee Ann Polytechnic, 535 Clementi Road, Singapore

Abstract

Tri-bore hollow fiber (HF) membranes with a triangular outer geometry were fabricated from polyvinylidene fluoride (PVDF) and explored for water deoxygenation. The representative membranes were hydrophobic and porous as seen from the contact angle of 94° and the porosity of 75%. The maximum load, elongation at break and the tensile stress of the tri-bore HF membranes were 3.90 N, 37.81% and 1.27 MPa, respectively, showing that prepared fibers were robust. The membranes were investigated for water deoxygenation, and mass transfer coefficients were found to be in the range of 1.89-7.40 × 10^{-5} m•s-1.Increasing the water flow rate resulted in higher deoxygenation efficiency under circulation mode but it almost did not influence the performance at one-pass mode. Operating temperature was observed to influence the deoxygenation in the early stage of the experiment and its influence was negligible after 30 min. The developed tri-bore HF membranes showed the potential for liquid degassing applications. Theoretical analysis disclosed that the resistance to the transport of oxygen across the membrane was mainly at the liquid water side.

Keywords: Tri-bore hollow fiber; Water deoxygenation; Mass transfer; Efficiency; Robust

Introduction

Dissolved oxygen (DO) needs to be carefully controlled in many production areas such as pharmaceuticals, food, power, biotechnology and semiconductors [1-4]. In semi-conductor industry, for instance, the presence of DO in ultrapure water, even at ppb level, facilitates the uncontrolled formation of silicon dioxide films and defects on wafers [1,5]. In the power industry, DO distinctly accelerates metal corrosion in the boiler or steel pipes [3]. DO in pharmaceutical and food production processes not only causes the corrosion of equipment but also favors the growth of bacteria, which deteriorate the lifetime of the products [6]. Consequently, water deoxygenation is extremely important in these industries.

Physical and chemical approaches as well as hybrid systems combining both approaches have been developed and used for DO control. Thermal and vacuum degassing are the most conventional physical methods and they have inherent drawbacks of high operating costs and bulky constructions [1]. Chemical approaches scavenge DO by the addition of reducing agents such as hydrazine or sodium sulfite. The reaction of reducing agents and DO generates solid products that are contaminants, and it brings environmental and safety hazards due to storing and handling chemicals [7]. Membrane contactor is an emerging technology for water deoxygenation. In a membrane contactor, separation of oxygen/water is accomplished through the membrane based on the concentration gradient of oxygen in water phase and in the gas phase with the gas phase under vacuum or sweeping with high-purity nitrogen [1,2,8]. Sinha and Li used commercial polypropylene (PP) membranes (Hoechst Celanese Corp.) assisted by nitrogen sweeping for DO removal from deionized (DI) water [4]. For the membrane contactors with areas below 0.1 m^2, the exiting DO concentration achieved was in the range of 0.3-0.8 ppm. At a water flow rate of 30 mL·min^{-1}, the exiting DO concentration could be reduced to below 1 ppm with a membrane area of 0.1 m^2 and 8 ppb with a membrane area of 0.4 m^2 [1]. Peng and his coworkers developed PP HF membranes, made pilot-scale membrane contactors and conducted deoxygenation testing [2]. The transverse flow of water at the shell side favored good performance. The membrane contactors were integrated with reverse osmosis (RO) system for water production and very stable DO removal efficiency was observed during the half-year test. For corrosion control by removing DO, Chung et al. used the membrane contactor (Hoechst Celanese Corp.) in the end-shield cooling system of a Nuclear Power Plant [9]. The DO removal efficiency observed was at 87-98% and it could be further enhanced with better vacuum, lower water flow rate

OPEN ACCESS

Correspondence:
Jincai Su, School of Life Sciences & Chemical Technology, Ngee Ann Polytechnic, 535 Clementi Road, Singapore.
E-mail: SU_Jincai@np.edu.sg

Received Date: 16 Nov 2017
Accepted Date: 15 Jan 2018
Published Date: 26 Jan 2018

Citation: Mao L, Wang F, Su J. Development of Robust Tri-Bore Hollow Fiber Membranes for the Control of Dissolved Oxygen in Water. SF J Material Chem Eng. 2018; 1(1): 1002.

ISSN 2643-8100

Table 1: Spinning conditions of TBF membranes.

Membrane ID	TBF-1	TBF-2	TBF-3	TBF-4	TBF-5
Polymer concentration (wt%)	12	13	15	15	17
Additive	PEG400 + LiCl (8 wt% + 2 wt%)	PEG400 + LiCl (5 wt% + 1 wt%)	PEG400 (5 wt%)	Nil	Nil
Dope flow rate (mL·min^{-1})	5	5	6	5	7
Bore fluid	NMP/water (50/50 wt%)	NMP/water (20/80 wt%)	NMP/water (20/80 wt%)	Water	Water
Bore flow rate (mL·min^{-1})	2.5	3	1.25	3	2
External coagulant	Water	Water	NMP/water (30/70 wt%)	Water	Water
Air-gap (cm)	1	1	15	10	10
Take up speed (m·min^{-1})	Free-fall				
Temperature (^{o}C)	25				
Room humidity (%)	65-75				

and higher water temperature. A transverse flow membrane contactor made with hydrophilic polysulfone HF membranes (X-Flow) was used by Vladisavljevic [10]. With nitrogen gas sweeping, 99.6% of the oxygen was removed from water and the exiting DO concentration was below 0.04 ppm. The mass transfer coefficient observed in this study was three orders of magnitude lower than that for hydrophobic PP membranes. Shao et al. used PP HF membranes (Shanghai Shenyu Sci. Cor.) for boiler feed water deoxygenation via vacuum degassing process [11]. Membrane fouling occurred and the foulants were mainly organic matter and aluminum silicate. Membrane contactors equipped with polyethylene and poly methyl pentene HF membranes were also used for water deoxygenation [12,13].

To achieve large surface area, the majority of membranes used in membrane contactors are single-bore HF with outer diameter in the range of 300-600 μm [2,4]. As well, high packing density is preferred. To be used for degassing RO or ultrapure water, the membrane contactors have shown excellent performance as discussed above. However, for water streams containing foulants, frequent air scouring and chemical cleaning are unavoidable [11]. It is quite common that slim fibers break and entangle one another during washing, shaking or mechanical cleaning [14-16]. Fiber breakage would cause entry of liquid water into the vacuum system, thus spoiling the deoxygenation operation. To minimize the influence of fiber breakage, multi-bore or composite HF membranes have been developed using polyethersulfone (PES), polyvinylidene fluoride (PVDF), polyacrylonitrile (PAN), ethylene vinyl alcohol (EVOH) copolymer and polyimide as raw materials for ultrafiltration, nanofiltration, forward osmosis and membrane distillation processes [17-28]. To date, there are no multibore HF membranes particularly designed for deoxygenation applications. The objective of this study was to develop tri-bore HF membranes with enhanced mechanical strength and capability for the removal of DO from water. The effects of operating conditions on the DO removal efficiency were studied and the mass transfer coefficient of deoxygenation was determined.

Experimental

Materials

Kynar HSV 900 PVDF supplied by Arkema Inc. was used for the fabrication of tri-bore HF membranes. N-methyl-2-pyrrolidone (NMP, 99.5%) and polyethylene glycol 400 (PEG400, >99.0%) used in membrane fabrication were supplied by Merck. Deionized (DI) water from Milli-Q (Millipore) system was used in all experiments.

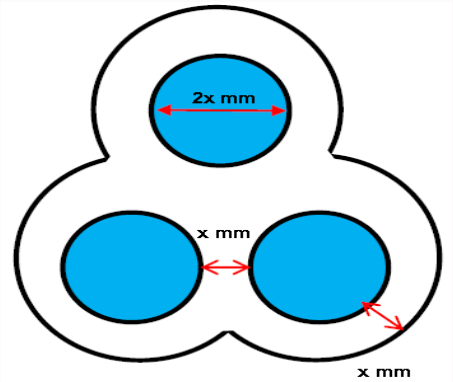

Figure 1: Schematic diagram of tri-needle spinneret.

Preparation of tri-bore HF membranes

Tri-bore HF membranes were fabricated via a dry-jet wet phase inversion spinning process as documented elsewhere [26]. The tri-bore spinneret used for spinning has three needles, which are distributed uniformly within the spinneret space as shown in Figure 1. A certain distance between channels is employed to avoid the potential intra-bore crossing of nascent fibers due to the dies well phenomena. For HF spinning, the dope solution and bore fluid were supplied at specified flow rates by ISCO syringe pumps (Teledyne, 1000D). After entering the coagulation bath, the nascent fibers precipitated and were collected by a take-up roller. Detailed spinning conditions are summarized in Table 1. After spinning, the as-spun tri-bore HF membranes were immersed in tap water for 2 days to completely remove the residual solvent and additives. The fibers were then frozen in a refrigerator and dried overnight in a freeze drier (S61-Modulyo-D, Thermo Electron).

Characterization of the membranes

Membrane morphology was inspected using a Field Emission Scanning Electron Microscope (FESEM, JEOL JSM-7600F). For FESEM inspection, membrane samples were fractured cryogenically in liquid nitrogen and coated with platinum using a sputtering coater (JEOL JFC-1600).

The membrane surface topology was examined using a Bruker

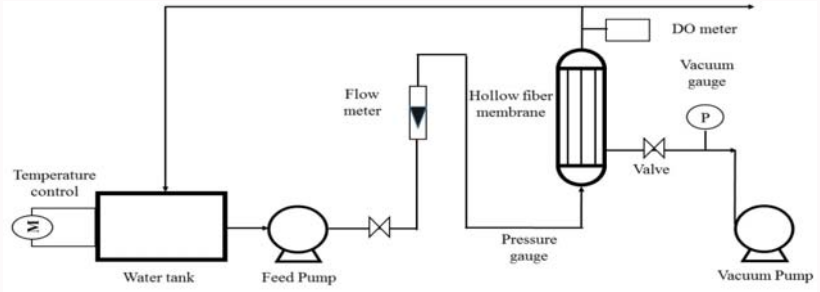

Figure 2: The schematic diagram of deoxygenation system.

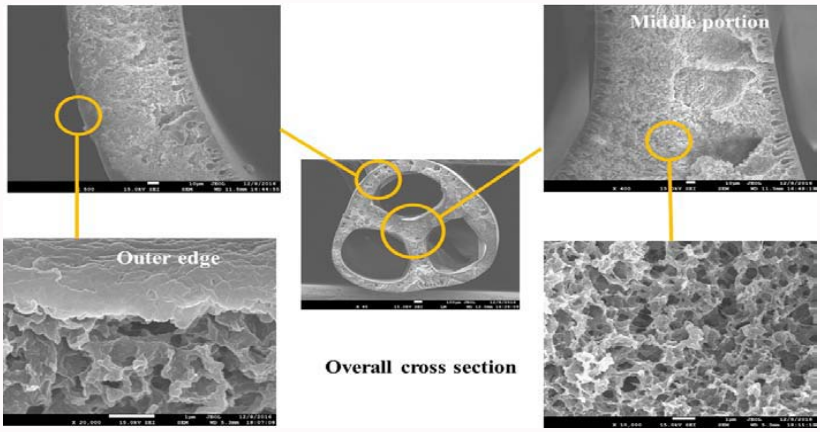

Figure 3: SEM images of tri-bore PVDF hollow fiber membrane TBF-3.

Dimension Icon Atomic Force Microscope (AFM). Small samples of the dried membranes (~0.5cm^2) were glued on a metal substrate. An area of 5×5 μm^2 was scanned using the tapping mode. Various roughness parameters such as the mean roughness (Ra), root mean square Z values (Rms), and maximum vertical distance between the highest and lowest data points (Rmax) were used to quantify the surface topology of the membranes.

Powder X-ray diffraction (XRD) patterns were investigated using a Bruker AXS X-ray powder diffractometer (D8 Advance, Cu Kα, λ=0.154060 nm). The fiber mechanical properties including the maximum load, elongation at break and tensile stress were examined using an Instron tensiometer (Model 3366, Instron Corp.) at room temperature. The starting gauge length was 50 mm, and a constant elongation rate of 10 mm·min^{-1} was applied. For each spinning condition, five fiber samples were tested and the average values were reported.

Dynamic contact angle of the outer surface of the fibers was measured using a Data physics DCAT21 tensiometer. Five measurements were made and the results were averaged for report.

The membrane porosity was measured by following the protocol described in [21]. Porosity ε is calculated from:

$$\varepsilon = \left(1 - \frac{m_{fiber} / \rho_{fiber}}{V_{fiber} - V_{channel}}\right) \times 100 \quad (1)$$

where m_{fiber} is the mass of fiber, ρ_{fiber} is the density of the fiber material (1.78 g·cm^{-3}), V_{fiber} is the fiber volume calculated from the fiber outer diameter and fiber length, and $V_{channel}$ is estimated from the fiber inner diameter and fiber length.

Experiments of do removal

The deoxygenation performance of the freeze-dried tri-bore HF membranes was evaluated through a lab-scale degassing system as shown in Figure 2. Prior to the tests, the membrane contactors were prepared by bundling the fibers into φ3/8 inch stainless steel tubing with the two ends sealed using epoxy resin. Every membrane contactor contained five pieces of fibers with an effective length of 91 cm. For the deoxygenation tests, DI water was pumped to the lumen side of the HF membranes while vacuum was applied on the shell side. Two operation modes were tried, i.e., single-pass and circulation. In the single-pass experiments, water was discharged directly after passing through the membrane contactor. In the circulation trials, 500 mL water was used and it flew back to the water tank after exiting from the membrane contactor. All the experiments were conducted at fixed temperatures controlled by using a water circulator (Julabo), and DI water was used to avoid the possible influence of membrane fouling. The efficiency (E) of deoxygenation is expressed as:

$$E = \left(1 - \frac{C_{out}^{l}}{C_{in}^{l}}\right) \times 100\% \quad (2)$$

where C_{in}^{l} and C_{out}^{l} are the DO concentrations in water at the inlet and outlet of the membrane contactor, respectively.

For deoxygenation experiments at the circulation mode, the experimental mass transfer coefficient (k_{exp}) could be determined by [12]:

$$\ln\left[\frac{C_t - C^*}{C_o - C^*}\right] = \frac{Q}{V}\left[\exp\left(-k_{exp} a \frac{L}{\omega}\right) - 1\right] \quad (3)$$

where C_0, C^* and C_t are the initial DO concentration, the DO

concentration that equilibrates with the gas phase within the membrane, and the remaining DO concentration at different experiment time, respectively, Q is the water flow rate, V is the volume of water in the tank, α is the membrane surface area to volume ratio, L is the length of the HF membranes, and ω is the water velocity. The value of C^* is estimated by using the Henry's law:

$$P_m = HC^* \quad (4)$$

where P_m is the average pressure within the membrane pore. At the one-pass mode, the experimental mass transfer coefficient k_{exp} is defined as [29]:

$$k_{\exp} = \frac{Q\left(C_{in}^l - C_{out}^l\right)}{A_m(\Delta C)lm} \quad (5)$$

where Q is the water flow rate, A_m is the inner surface area of the HF membranes and $(\Delta C)_{lm}$ is the logarithmic mean concentration difference of DO. $(\Delta C)_{lm}$ is defined as:

$$(\Delta C)_{lm} = \frac{\left(C_{in}^l - C^*\right) - \left(C_{out}^l - C^*\right)}{\ln\left[\left(C_{in}^l - C^*\right)/\left(C_{out}^l - C^*\right)\right]} \quad (6)$$

Theory

The mass transfer in vacuum deoxygenation involves the diffusion of oxygen in liquid water, membrane pores, and surrounding vacuum or gas stream [12,30]. The sum of the resistance defines the overall resistance to gas transfer within a membrane contactor, as shown in the equation below

$$\frac{1}{K_{cal}} = \frac{1}{k_l} + \frac{1}{Hk_m} + \frac{1}{Hk_g} \quad (7)$$

where k_l, k_m, and k_g are the mass transfer coefficients in the liquid water, across the membrane and in the gas film layer, respectively, and H is a Henry's law constant. Water always flows at the lumen side of the tri-bore HF membranes in this study. Since the shell side is kept at vacuum, the resistance in the gas film layer is negligible.

Empirically, the mass transfer coefficient in the liquid water within the membrane contactor can be expressed using Sherwood, Reynolds and Schmidt numbers as below [30,31]:

$$Sh = 1.85\left(\mathrm{Re}\,Sc\frac{d_e}{L}\right)^{0.33} \quad (8)$$

$$Sh = k_l\frac{d_e}{D} \quad (9)$$

$$\mathrm{Re} = \frac{d_e\omega\rho}{\mu} \quad (10)$$

$$Sc = \frac{\mu}{\rho D} \quad (11)$$

where d_e is the equivalent diameter of the liquid water flow channel within the membrane contactor, μ is viscosity, D is the diffusivity of oxygen within the liquid water and ρ is the density of water. Oxygen molecules passing thorough the porous PVDF tri-bore HF membranes involve Knudsen diffusion or viscous flow, but the former may be dominant based on the fact that the pores of the membranes are around 100 nm. Knudsen number (K_n) is defined as the ratio of the mean free path (λ) of the oxygen molecule to the pore diameter of the membrane (d_p):

$$K_n = \frac{\lambda}{d_p} \quad (12)$$

The mean free path of oxygen molecules can be calculated by the following equation [32]:

$$\lambda = \frac{k_B T}{\sqrt{2}\pi p_m \sigma_w^2} \quad (13)$$

where k_B is the Boltzmann constant and σ_{O2} is the collision diameter of oxygen. In the case of K_n>10 or d_p<0.1λ, the collision between oxygen molecules and the pore wall is dominant over the collision between oxygen molecules [33]. Therefore, the transport of oxygen molecules is mainly through Knudsen diffusion and the mass transfer coefficient across the membrane can be expressed as:

$$k_{m,kn} = \frac{2}{3}\left(\frac{8M_w}{\pi RT}\right)^{0.5}\frac{\varepsilon r_p}{\delta\tau} \quad (14)$$

where ε, r_p, δ and τ are the porosity, pore radius, thickness and pore tortuosity of the membrane, respectively, M_w is the molecular weight of oxygen, R is the gas constant and T is the absolute temperature. When K_n< 0.01 or d_p>100λ, the mean free path of oxygen molecules is negligible compared to the pore dimension and the collisions between oxygen molecules dominate. For this case, the viscous flow exists and the mass transfer coefficient across the membrane can be determined by

$$k_{m,vis} = \frac{1}{8\eta}\frac{\varepsilon r_p^2}{\delta\tau}\frac{M_w P_m}{RT} \quad (15)$$

where η is the viscosity of oxygen. When 0.01<K_n<10, both Knudsen flow and viscous flow exist and the combined mass transfer coefficient across the membrane is

$$k_m = k_{m,Kn} + k_{m,vis} = \frac{2}{3}\left(\frac{8M_w}{\pi RT}\right)^{0.5}\frac{\varepsilon r_p}{\delta\tau} + \frac{1}{8\eta}\frac{\varepsilon r_p^2}{\delta\tau}\frac{M_w P_m}{RT} \quad (16)$$

Results and Discussion

General characteristics of the membranes

All the five groups of TBF membranes have similar triangular outer geometry with three round bores evenly distributed in the center. Using TBF-3 as an example, the typical morphology of TBF membranes is shown in Figure 3. The TBF-3 fiber has relatively dense skin at the inner and outer walls because both the bore fluid and external coagulant used for the spinning contain high percentage of water, i.e., 80 wt% and 70 wt%, respectively. Such double-skin structure is able to protect the membrane from pore blockage by suspended solids either running the feed water at the shell or lumen side. The TBF-3 fiber has a wall thickness of around 120 μm with an average diameter of the inner bore channels around 760 μm. Compared with multi-bore HF with a round geometry, this triangular configuration offers a relatively more uniform fiber wall thickness which favors mass transport and higher ratio of inner surface to fiber cross-section area [27]. A layer of finger-like macro voids could be found near the inner edges of the fibers probably due to the rapid phase inversion and nonsolvent (i.e., water) intrusion [20,34-36]. While a sponge-like porous structure is formed close to the outer surface owing to the delayed demixing, i.e., the solvent-nonsolvent exchange being retarded by the outer skin formed [20,37,38].

Figure 4 illustrates the inner and outer surface morphologies of TBF membranes fabricated from different spinning conditions. Based on 12 and 13 wt% polymer concentrations and NMP/water bore

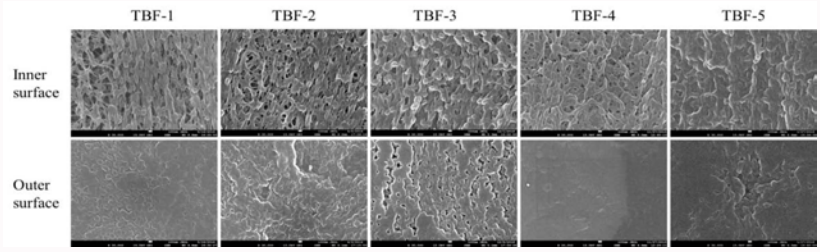

Figure 4: SEM images of tri-bore HF membranes under different spinning conditions.

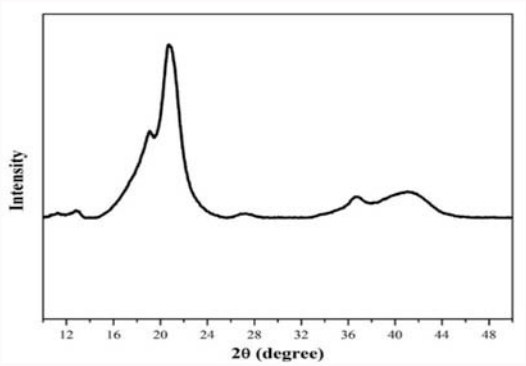

Figure 5: XRD patterns of tri-bore hollow fiber membrane TFB-3.

fluid, TBF-1 and TBF-2 membranes have porous inner surface. When the polymer concentration increases to 15 wt%, the inner surface of TBF-3 and TBF-4 membranes is less porous no matter NMP/water or water is used as the bore fluid. A polymer concentration of 17 wt% and the bore fluid of water result in dense inner surface. For all the membrane samples fabricated using water as the external coagulant, the outer surface is relatively tighter, consisting of interconnected globules with different degrees of interconnectivity. The only membrane sample having porous outer surface is TBF-3, which is fabricated using NMP/water (30/70 wt%) as the external coagulant. It should be also noted that longer air-gap distance of 15 cm was used for the fabrication of the TBF-3 membrane. Appropriate stretching after the nascent fibers are extruded from the spinneret might also contribute to its porous structure. Poor spinnability was observed for the dope solutions containing relatively low concentration of polymer (e.g., 12 or 13 wt%). Adding LiCl could increase the viscosity of the dope solutions, but the amount of LiCl has to be carefully controlled because it reduces the solubility of PVDF in NMP. Porous structure is preferable for water deoxygenation and this is why PEG400 is used as pore former. However, the dope solution tends to gel and is difficult to spin if the PEG concentration reaches 7 wt%. Considering the spinnerability and preferable membrane structure, the characterization and deoxygenation tests are mainly focused on the TBF-3 membrane.

Table 2 summarizes the general characteristics of the as-spun tri-bore TBF-3 HF membranes. The membranes have a porosity of 75% which is beneficial for the fast transport of oxygen. A water contact angle of 94° indicates the necessary hydrophobicity, which helps to prevent the liquid water from entering the membrane pores at operating pressure. It should be noted that the contact angle was measured for the fiber outer surface. The tri-bore HF membranes exhibit excellent stretchability in view of the elongation at break about 3-5 times higher than multibore hollow fibers reported previously [20,21,26,27]. The maximum load is about 2-3 times higher than that of single-bore PVDF HF membranes fabricated based on a similar formulation.

Figure 5 shows the X-ray diffraction pattern of the membrane. The strong peak at 2θ=20.7°, assigned to the reflection of the (200) and (100) planes, and weak peaks at 36.6 and 42.2° are the characteristics of β phase crystal structure of PVDF [39]. The two-dimensional AFM image shown in Figure 6a clearly illustrates the porous structure of the membrane inner surface. As seen from the three-dimensional AFM image in Figure 6b, a large number of very tiny nodules exist at the inner surface. This is an indication that the membrane offers high contact area, which is favorable for accelerated mass transport [Gekas and Olund, 1988] [40]. The mean roughness (Ra) of the inner surface is 34.9 nm and the root mean square value (Rms) is 44.7 nm. The maximum vertical difference between the highest and lowest data points (Rmax) is 365 nm, indicating a moderate roughness [41].

Performance for water deoxygenation

The deoxygenation performance of the membrane contactors packed with tri-bore HF membranes was studied under a vacuum condition of around 3000 Pa. Figure 7 presents the deoxygenation performance at different flow rate at the circulation mode. At the room temperature of 21°C, DI water is saturated with oxygen at about

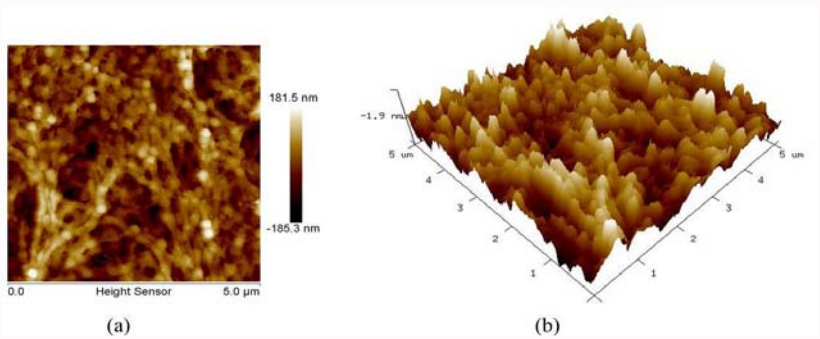

Figure 6: AFM images of the inner surface of the TBF-3 membrane: (a) two-dimensional image and (b) three-dimensional image.

Table 2: Characteristic properties of the TBF-3 membrane.

Membrane	Inner diameter (μm)	Maximum load (N)	Elongation at break (%)	Tensile stress (MPa)	Porosity (%)	Water contact angle (°)
TBF-3	760	3.03	37.81	1.27	75	94

Table 3: Experimental mass transfer.

Membrane	k_{exp}(×10^5 m·s^{-1})*		
	12°C	21°C	40°C
TBF-3	2.19	2.43	2.43

* Water circulation rate: 100 mL·min^{-1}

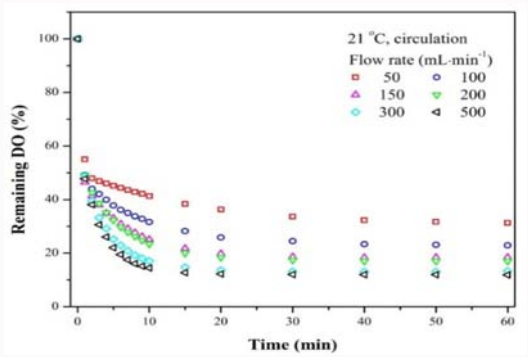

Figure 7: Effect of the water flow rate on the deoxygenation performance of TBF-3 at the circulation mode.

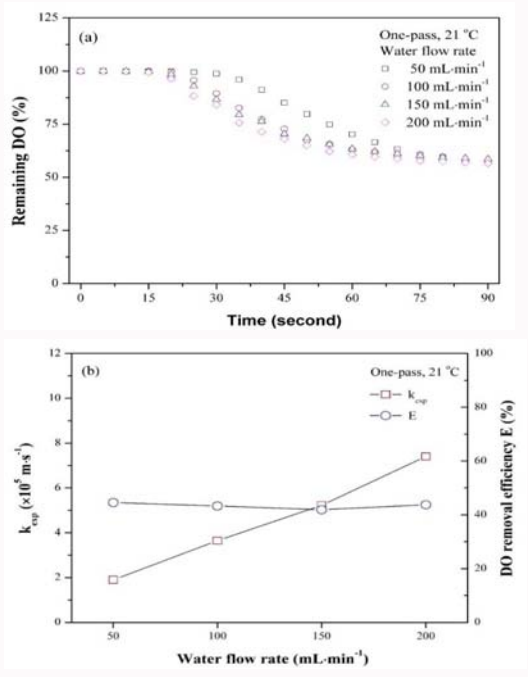

Figure 8: Effect of the water flow rate on the deoxygenation performance of TBF-3 at the one-pass mode: (a) Remaining DO vs. time and (b) Experimental mass transfer coefficient and DO removal efficiency.

8.89 ppm and it is the initial DO level presented as 100%. An obvious drop of the DO level can be seen in the first few minutes and the decline becomes slow afterwards. For each water flow rate, the DO level is almost constant after 30 minutes. With increasing the water flow rate, DO is removed faster and the final DO concentration is lower. At a flow rate of 500 mL·min^{-1}, the lowest DO concentration of 1.05 ppm in the product water is achieved and this corresponds to a DO removal percentage of 88.19% (remaining DO of 11.81%). The

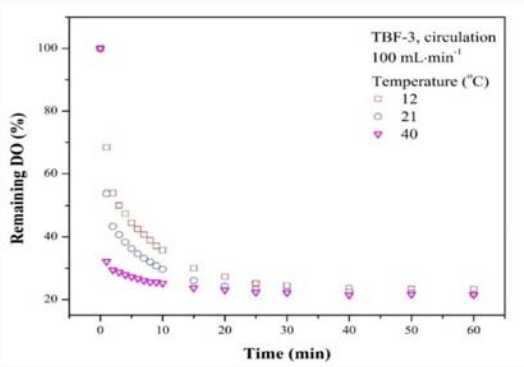

Figure 9: Deoxygenation performance of the TBF-3 membrane at different temperatures.

relatively high DO removal ability is consistent with the morphology analyses discussed above. The remaining DO concentrations are in the range of 1.07-2.99 ppm after 30min deoxygenation test. It should be noted that the DO removal efficiency is not as high as those reported in previous studies such as Peng et al. (DO removal efficiency of 89.2-97.5%) due to the much smaller membrane area and non-optimized experimental conditions [2,12,29].

At the one-pass mode, the outlet DO changes with the water flow rate in the first 90 seconds and it is almost identical subsequently as shown in Figure 8a. Eventually, the DO removal efficiency is not very different although the mass transfer is enhanced during a short period of time with increasing the water flow rate (Figure 8b). It is not surprising that k_{exp} has same values after 90 seconds. This is different from previous observations at the same operation mode, i.e., higher flow rate usually giving rise to a higher mass transfer coefficient but a lower DO removal efficiency [2,8]. The possible reason is that the flow rate used in this study is relatively low due to the limitation from the experimental facility and its change is also small. Higher mass transfer coefficient at a faster water flow rate is reasonable because the resistance for the oxygen transport mainly lies in the liquid phase while the change in hydraulic conditions does affect the mass transfer rate within the water boundary layer at the membrane surface.

The influence of operating temperature on the deoxygenation performance was studied at the circulation mode at 100 mL·min^{-1} (Figure 9). The remaining DO level drops faster in the first 15 min at higher temperatures. After 30 min, the remaining DO concentrations are close to each other and are almost independent on the temperature. Obviously, the solubility of oxygen in water drops when the temperature increases and its diffusion is faster. This might explain the DO change observed at the early stage of the experiments. k_{exp} has values of 2.19×10^{-5}, 2.43×10^{-5} and 2.43×10^{-5} m·s^{-1} at temperatures of 12, 21 and 40°C, respectively, for the tri-bore HF membranes (Table 3). It can be extrapolated that the solubility and the diffusion rate of DO in the bulk water do not significantly influence the overall mass transfer. When the deoxygenation is conducted at the one-pass mode, k_{exp} increases from 1.90×10^{-5} to 3.64×10^{-5}, 5.22×10^{-5} and 7.40×10^{-5} m·s^{-1} when the water flow rate is increased from 50 to 100, 150 and 200 mL·min^{-1}, respectively, in the initial stage of experiment. The mass transfer coefficients observed for the tri-bore HF membranes are in

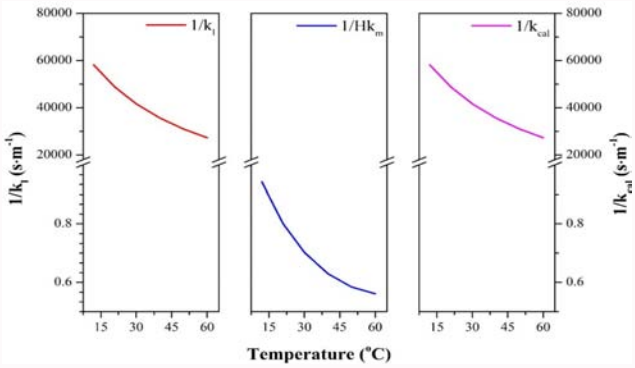

Figure 10: Effect of operating temperature on the mass transfer through the TBF-3 membrane.

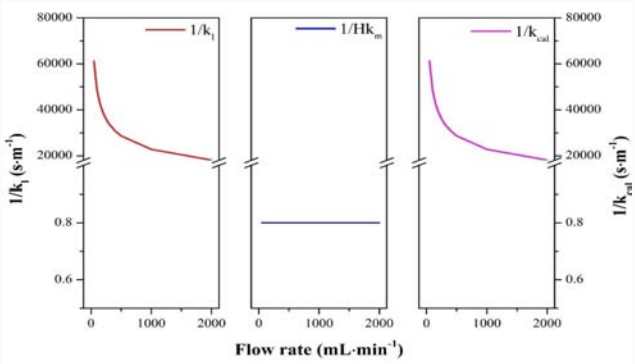

Figure 11: Effect of the water flow rate on the mass transfer of the TBF-3 membrane.

the same range as those reported in other studies [2,13].

To further understand the transport of oxygen across the membrane, equations 7-16 were used to calculate the theoretical mass transfer coefficient. With increasing the water temperature, the resistance at the liquid side decreases significantly due to decreased water viscosity and increased oxygen diffusivity within the boundary layer (Figure 10). It is observed that at different temperatures, vacuum levels or water flow rates, K_n always has values above 100 while $k_{m,Kn}$ is 10-300 times higher than $k_{m,vis}$. Therefore, Knudsen diffusion dominates the transport of oxygen across the membrane. The resistance to oxygen transport through the membrane increases at enhanced temperatures due to higher viscosity of oxygen as well as more vigorous collisions between oxygen molecules and the membrane pore wall. Nevertheless, the resistance contributed by the membrane is still much lower than that from the liquid phase. Increasing the water flow rate favors the overall mass transfer coefficient while the influence becomes smaller when the water flow rate is above 500 mL·min^{-1} (Figure 11). It is noted that water is at laminar flow at the experimental conditions in this study. Still, the resistance created by the membrane is low and negligible. The increase in the water flow rate enhances the transport of oxygen through the water boundary layer at the membrane surface, but the corresponding resistance is still more than 20000 thousands time of that in the membrane phase. Improving the vacuum at the membrane shell side only slightly decreases the mass transfer resistance across the membrane (Figure 12). However, its influence is very small and the overall resistance is almost unchanging. It could be concluded that the deoxygenation through the tri-bore HF membranes is dominated

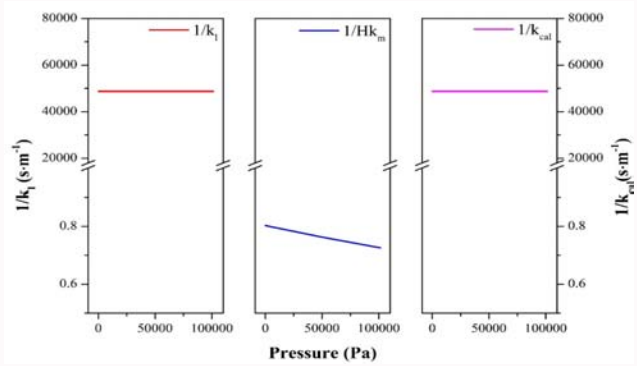

Figure 12: Effect of the vacuum on the mass transfer of the TBF-3 membrane.

by the mass transfer at the liquid water side. This is consistent with the observations by Leiknes and Semmens for single-bore HF membranes [12]. The above analyses provide valuable guidance for the further development of tri-bore HF membranes, i.e., to optimize the membrane surface characteristics such as roughness, number of pores, and surface chemistry in order to enhance the mass transfer rate.

Conclusions

- In this study, novel tri-bore PVDF HF membranes were developed for water deoxygenation applications. The physiochemical properties of the membranes and their deoxygenation performance under different conditions were studied. The following conclusions canTriangular shape tri-bore PVDF HF membranes were prepared using a tri-bore blossom spinneret. The as-spun PVDF membranes mainly contained β-phase crystal, exhibiting a porous inner surface and a relatively tight outer surface.

- The tri-bore HF membranes exhibited excellent mechanical strength. The maximum load, elongation at break, and tensile stress could reach 3.90 N, 37.81% and 1.27 MPa. Therefore, the tri-bore HF membranes would have enough mechanical strength to resist the pressure from the water flow in real applications.

- The as-prepared membranes showed a porosity of 75% and a water contact angle of 94°, making them a good candidate for the water deoxygenation and even other water degassing purposes.

- The DO removal rate could be enhanced with the increase in the water flow rate and the operating temperature. Theoretical analyses were consistent with the experimental observations.

- Further investigations would be needed at enlarged scale. Pilot testing is ongoing and will be reported in the future.

Acknowledgments

This work was financially supported by the Singapore Ministry of Education (grant number MOE2014-TIF-1-G-020). The authors are thankful to Professor Tai-Shung Chung and his team members (National University of Singapore) for providing the facilities and valuable suggestions.

References

1. Tai MSL, ChuaI Li K, Ng WJ and Teo WK. Removal of dissolved oxygen in ultrapure water production using microporous membrane modules. J Membr Sci. 1994; 87: 99–105.

2. Peng ZG, Lee SH, Zhou T, Shieh JJ and Chung TS. A study on pilot-scale

degassing by polypropylene (PP) hollow fiber membrane contactors. Desalination. 2008; 234: 316–322.

3. Mahdizadeh F and Eskandarian M. Glucose oxidase and catalase co-immobilization on biosynthesized nanoporous SiO_2 for removal of dissolved oxygen in water: Corrsion controlling of boilers. J Ind Eng Chem. 2014; 20: 2378–2383.

4. Sinha V and Li K. Alternative methods for dissolved oxygen removal from water: a comparative study. Desalination. 2000; 127: 155–164.

5. Sato H, Hashimoto N, Shinoda T and Takino K. In Proceedings of the 10th Annual Semiconductor Pure Water Conference; Balazs MK Ed. Dissolved oxygen removal in ultrapure water for semiconductor processes, in Proceedings of the 10th Annual Semiconductor Pure Water Conference. Santa Clara, CA. 1991: 147.

6. Degenhardt OS, Waters B, Rebelo-Cameirao A, Meyer A, Brunner H and Toltl NP. Comparison of the effectiveness of various dearation techniques. Dissolution Technol. 2004; 11: 1–6.

7. Tan X, Capar G and Li K. Analysis of dissolved oxygen removal in hollow fiber membrane modules: effect of water vapour. J Membr Sci. 2005; 251: 111–119.

8. Ito A, Yamagiwa K, Tamura M and Furusawa M. Removal of dissolved oxygen using non-porous hollow fiber membranes. J Membr Sci. 1998; 145: 111–117.

9. Chung KH, Kang DW and Hong SY. Removal of dissolved oxygen forms the make-up water of NPP using membrane-based oxygen removal system. Korean Nuclear Soc. 1999; 31: 541–547.

10. Vladisavljevic GT. Use of polysulfone hollow fibers for bubbleless membrane oxygenation/deoxygenation of water. Sep Purif Technol. 1999; 17: 1–10.

11. Shao J, Liu H and He Y. Boiler feed water deoxygenation using hollow fiber membrane contactor. Desalination. 2008; 234: 370–377.

12. Leiknes T and Semmens MJ. Vacuum degassing using microporous hollow fiber membranes. Sep Purif Technol. 2000; 22-23: 287–294.

13. Kartohardjono S, Chen V and Leiknes T. The Fifth International Membrane Science and Technology Conference (IMSTEC'03); November 10–14, 2003. Dissolved oxygen removal form water by vacuum degassing process using sealed end poly methyl pentene (PMP) hollow fiber membranes contactor. The Fifth International Membrane Science and Technology Conference (IMSTEC'03).The University of New South Wales, Sydney, Australia.

14. Gijsbertsen-Abrahamse AJ, Cornelissen ER and Hofman JAMH. Fiber failure frequency and cause of hollow fiber integrity loss. Desalination. 2006; 194: 251–258.

15. Tng KH, Antony A, Wang Y and Leslie GL. Membrane ageing during water treatment: Mechanisms, monitoring, and control in Advances in membrane technologies for water treatment. Elsevier Ltd. 2015; 349–378.

16. Le-Clech P, Fane A, Leslie G and Childress A. MBR focus: the operators' perspective. Filtr Sep. 2005; 42: 20–23.

17. Kruger R, Vial D, Buchta P and Winkler R. Use of innovative inge® Multibore® ultrafiltration membranes for the treatment of challenging seawater. Desalination and Water Treatment. 2016; 57: 22902–22908.

18. Gille D and Czolkoss W. Ultrafiltration with multi-bore membranes as seawater pre-treatment. Desalination. 2005; 182: 301–307.

19. Bu-Rashid KA and Czolkoss W. Pilot tests of Multibore UF membrane at Addur SWRO, Desalination Plant, Bahrain. Desalination. 2007; 203: 229–242.

20. Wang P and Chung TS. A new generation asymmetric multi-bore hollow fiber membrane for sustainable water production via vacuum membrane distillation. Environ Sci Technol. 2013; 47: 6272–6278.

21. Wang P and Chung TS. Design and fabrication of lotus-root-like multi-bore hollow fiber membrane for direct contact membrane distillation. J Membr Sci. 2012; 421–422: 361–374.

22. Teoh MM, Peng N, Chung TS and Koo LL. Development of novel multichannel rectangular membranes with grooved outer selective surface for membrane distillation. Ind Eng Chem Res. 2011; 50: 14046–14054.

23. Peng N, Teoh MM, Chung TS and Koo LL. Novel rectangular membranes with multiple hollow holes for ultrafiltration. J Membr Sci. 2011; 372: 20–28.

24. Bonyadi S and Mackley M. The development of novel micro-capillary film membranes. J Membr Sci. 2012; 389: 137–147.

25. Spruck M, Hoefer G, Fili G, Gleinser D, Ruech A, Schmidt-Baldassari M et al. Preparation and characterization of composite multichannel capillary membranes on the way to nanofiltration. Desalination. 2013; 314: 28–33.

26. Wang P, Luo L and Chung TS. Tri-bore ultra-filtration hollow fiber membranes with a novel triangle-shape outer geometry. J Membr Sci. 2014; 452: 212–218.

27. Luo L, Wang P, Zhang S, Han G and Chung TS. Novel thin-film composite tri-bore hollow fiber membrane fabrication for forward osmosis. J Membr Sci. 2014; 461: 28–38.

28. Zuo J, Chung TS, O'Brien GS and Kosar W. Hydrophobic/hydrophilic PVDF/Ultem® dual-layer hollow fiber membranes with enhanced mechanical properties for vacuum membrane distillation. J Membr Sci. 2017; 523: 103–110.

29. Bhaumik D, Majumdar S, Fan Q and Sirkar KK. Hollow fiber membrane degassing in ultrapure water and micro biocontamination. J Membr Sci. 2004; 235: 31–41.

30. Yang MC and Cussler EL. Designing hollow-fiber contactors. AlChE J. 1986; 32: 1910–1916.

31. Ahmed T and Semmens MJ. The use of independently sealed microporous hollow fiber membranes for oxygenation of water: model development. J Membr Sci. 1992; 69: 11–20.

32. Thomson GWM. The antoine equation for vapor-pressure data. Chem Rev. 1946; 38: 1–39.

33. Yang Y, Rana D, Matsuura T and Lan CQ. The heat and mass transfer of vacuum membrane distillation: Effect of active layer morphology with and without support material. Sep Purif Technol. 2016; 164: 56–62.

34. Peng N, Chung TS and Wang KY. Macro void evolution and critical factors to form macro void-free hollow fiber membranes. J Membr Sci. 2008; 318: 363–372.

35. Strathmann H and Kock K. The formation mechanism of phase inversion membranes. Desalination. 1977; 21: 241–255.

36. Horibe H and Taniyama M. Poly (vinylidene fluoride) crystal Structure of poly (vinylidene fluoride) and poly (methyl methacrylate) blend after annealing. J The Electrochem Soc. 2006; 153: G119–G124.

37. Smolders CA, Reuvers AJ, Boom RM and Wienk IM. Microstructures in phase-inversion membranes. Part I. Formation of macro voids. J Membr Sci. 1992; 73: 259–275.

38. Wienk IM, Boom RM, Beerlage MAM, Bulte AMW and Smoders CA. Recent advances in the formation of phase inversion membranes made from amorphous or semi-crystalline polymers. J Membr Sci. 1996; 113: 361–371.

39. Sukitpaneenit P and Chung TS. Molecular design of the morphology and pore size of PVDF hollow fiber membranes for ethanol–water separation employing the modified pore-flow concept. J Membr Sci. 2011; 374: 67–82.

40. Gekas V and Olund K. Mass transfer in the membrane concentration polarization layer under turbulent cross flow. II. Application to the

characterization of ultrafiltration membranes. J Membr Sci. 1988; 37: 145–163.

41. Khulbe KC, Feng C, Matsuura T, Kapantaidakis GC, Wessling M and Koops GH. Characterization of polyethersulfone-polyimide hollow fiber membranes by atomic force microscopy and contact angle goniometery. J Membr Sci. 2003; 226: 63–73. be drawn: